PALEOCEANOGRAPHY, VOL. 16, NO. 5, PAGES 491–502, OCTOBER 2001

Millennial-scale dynamics of the East Asian winter monsoon during the last 200,000 years

Thibault de Garidel-Thoron and Luc Beaufort
Centre Européen de Recherche et d'Enseignement en Géosciences de l'Environnement (CEREGE), Aix-en-Provence, France

Braddock K. Linsley and Stefanie Dannenmann
Department of Earth and Atmospheric Sciences, University at Albany, State University of New York, Albany, New York, USA

Abstract. The primary productivity dynamics of the last 200,000 years in the Sulu Sea was reconstructed using the abundance of the coccolithophore *Florisphaera profunda* in the IMAGES MD97-2141 core. We find that primary productivity was enhanced during glacial periods, which we suggest is due to a stronger East Asian winter monsoon. During the last 80 kyr, eight significant increases in primary productivity (PP) in the Sulu Sea are similar to East Asian winter monsoon changes recorded in Chinese loess. The PP maxima are not linked with Heinrich events (HE) in the North Atlantic, although four PP peaks are synchronous with HE. The PP oscillations have frequencies near those of the Dansgaard–Oeschger cycles in Northern Hemisphere ice records and indicate a teleconnection of the East Asian winter monsoon with Greenland climate. In this Sulu Sea record the East Asian winter monsoon oscillates with periodicities of ~6, 4.2–3.4, 2.3, and 1.5 kyr. In particular, the 1.5 kyr cycle exhibits a strong and pervasive signal from stage 6 to the Holocene without any ice volume modulation. This stationarity suggests that the 1.5 kyr cycle is not driven by some high-latitude forcing.

1. Introduction

The coupling between the atmosphere and the ocean is fundamental to climate dynamics over seasonal to millennial timescales. Variations in this coupling influence the oceanic biosphere and particularly the phytoplankton of the upper ocean layer. In low-latitude areas the phytoplanktonic activity quantified by primary productivity (PP) is correlated to the wind stress dynamics on the sea surface [*Nair et al.*, 1989]. Previous studies have concentrated on long-term changes in the PP [e.g., *Beaufort et al.*, 1997; *Mix*, 1989], but little is known about the millennial-scale dynamics of PP.

At present, we know that during the last glacial stage our climate system went through rapid changes that are well documented in the North Atlantic area. Two major types of abrupt changes have been described. Heinrich events are documented massive iceberg discharges of ice-rafted debris to the North Atlantic deep-sea sediments occurring with a periodicity of ~6–7 kyr [*Bond et al.*, 1992; *Heinrich*, 1988]. These events are followed by consecutive abrupt warmings on the Greenland continent. Dansgaard–Oeschger (D–O) climatic oscillations with periods of 1000–3000 years have been described in the Greenland ice cores records [*Dansgaard et al.*, 1993]. These oscillations correspond to ~15°C air temperature shifts between a stadial (cold phase) and an interstadial (warm phase) [*Jouzel*, 1999].

The Heinrich events are correlative with major changes in the climate dynamics recorded worldwide, from the North Atlantic to the Antarctic. In the Asian region the East Asian winter monsoon strengthened during Heinrich events [*Porter and Zhisheng*, 1995; *Xiao et al.*, 1999]. Planktonic foraminifera assemblages in South China Sea recorded these abrupt changes [*Chen and Huang*, 1998; *Wang et al.*, 1999]. In the Sulu Sea the oxygen isotopes ($\delta^{18}O$) of planktonic foraminifera show important rapid oscillations which appear synchronous with some Heinrich events [*Linsley*, 1996].

For the Dansgaard–Oeschger oscillations recorded in ice cores, similar changes are documented in sea surface temperature (SST) reconstructions, percentage of carbonate, magnetic susceptibility, planktonic foraminifera oxygen isotopic composition, and foraminiferal assemblage records from the North Atlantic Ocean (for a review, see *Cortijo et al.* [2000]). The loess-paleosol record in China exhibits comparable shifts [*Chen et al.*, 1997]. In the Santa Barbara basin a bioturbation index records nearly all stadials and interstadials described in the Greenland record [*Behl and Kennet*, 1996]. At low latitudes, organic carbon changes in the Arabian Sea appear to correlate with D-O cycles [*Schulz et al.*, 1998].

To constrain the past millennial variations of low-latitude paleoproductivity, we investigate, at high-resolution, variations in the coccolith assemblages in IMAGES giant piston core MD97-2141 located in the Sulu Sea (Figure 1).

The Sulu Sea is located between the Asian continent and the "Western Pacific Warm Pool" (WPWP), where annual SST is above 29°C [*Yan et al.*, 1992]. The climate of the Sulu Sea is strongly influenced by the East Asian monsoon. The East Asian monsoon results from the different potential heating between the WPWP and the Asian continent. During the boreal winter the main heating source is located in the ocean. The latent heat release associated with intense convective precipitation fuels the meridional circulation. Tropical convection in the western equatorial Pacific is connected to the descending branch over the Siberian region, forming a strong local Hadley cell in the East Asian region [*Zhang et al.*, 1997]. The East Asian winter monsoon winds in the Sulu Sea result from the merging of the northerly East Asian monsoon with the Pacific trade winds over the South China Sea [*McGregor and Nieuwolt*, 1998]. East Asian winter monsoon bursts during January to March (Figure 2) can induce blooms of coccolithophorids [*Wiesner et al.*, 1996]. The PP rises correlatively to the wind stress strengthening because of the stronger mixing of the upper ocean (Figure 2) [*Nair et al.*, 1989]. Thus coccolith

Paper number 2000PA000557.
0883-8305/01/2000PA000557$12.00

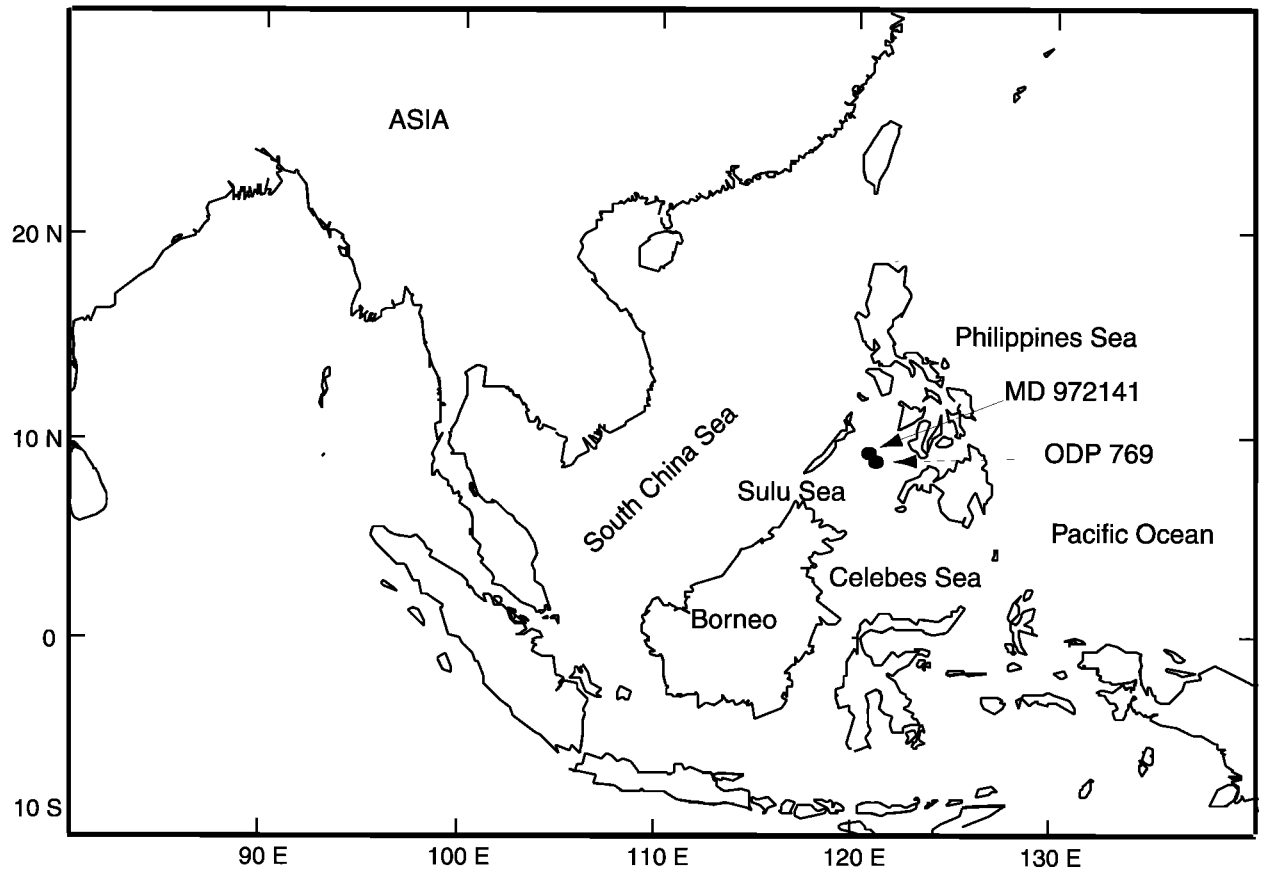

Figure 1. Map of Southeast Asia and of the marginal seas of the western Pacific. Note location of core MD97-2141 in the Sulu Sea.

assemblages record information on both paleoproductivity changes and also on East Asian winter monsoon variations in the Sulu Sea.

2. Material

The 36 m giant piston core IMAGES MD97-2141 (08°47′N, 121°17′E, 3633 m depth) was retrieved during the IPHIS-IMAGES III cruise of the R/V *Marion Dufresne* in May 1997. This position is located in the vicinity of the Ocean Drilling Program (ODP) Site 769 [*Linsley*, 1996]. The core is located on the Cagayan ridge, which protects the site from downslope processes, and above the present lysocline depth (~3800 m), allowing for good preservation of carbonates [*Linsley et al.*, 1985; *Miao et al.*, 1994]. The sediments are composed predominantly of well-preserved nannofossil-foraminifera oozes.

3. Methods

For coccolith counting, the core was sampled every 2 cm in the upper 6 m of the core, allowing for a resolution of ~70 years, and every 3–4 cm in the lower 30 m for a resolution of ~200–500 years. A smear slide was prepared for each sample, and at least 300 coccoliths were counted for each slide (mean of 357 coccoliths) on a Zeiss Axioscop at a 1000× resolution. Percentages of *Florisphaera profunda* (Fp) were computed using the following equation:

$$\%\mathrm{Fp} = 100(\mathrm{numberFp})/(\mathrm{totalcoccoliths})$$

The 95% confidence interval for %Fp varies between ±2 and ±6% depending on the percentage of Fp [*Patterson and Fishbein*, 1989].

3.1. Age Model

The age model of the core MD97-2141 was developed by *Dannenmann et al.* [1998] and *Oppo et al.* [1998]. It was obtained using 28 accelerator mass spectrometer (AMS) ^{14}C ages on *Globigerinoides ruber* and *G. sacculifer* and by comparison of the planktonic foraminifera δ^{18}O curve (on *Globigerinoides ruber* and *G. sacculifer* tests) with the SPECMAP stack [*Imbrie et al.*, 1984] (Table 1). The radiocarbon dates were converted to calendar ages using (1) a correction of 400 years, according to the age reservoir of carbon in the ocean [*Bard*, 1988], and then (2) the CALIB3 calibration software [*Stuiver and Reimer*, 1993] to take into account past atmospheric changes in cosmogenic production. All the ages discussed here are calendar ages B.P. The carbon reservoir age in this work is assumed to be invariant with time. We also assumed that the carbon reservoir age changes in the tropical upper oceanic layer where *G. ruber* and *G. sacculifer* live are not varying more than ~200 years [*Duplessy et al.*, 1991]. The last appearance datum of *G. ruber* pink at 1593 cm fits with the Termination II [*Thompson et al.*, 1979], strengthening the validity of the age model (Figure 3). Two ninth-order polynomial regressions were used from the core top to 400 cm and from 440 to 920 cm on the ^{14}C ages and SPECMAP tie points to smooth the sedimentation rate for the last 60 kyr. This smoothing is indispensable for the spectral analyses to avoid spurious peaks linked with sedimentation rates changes.

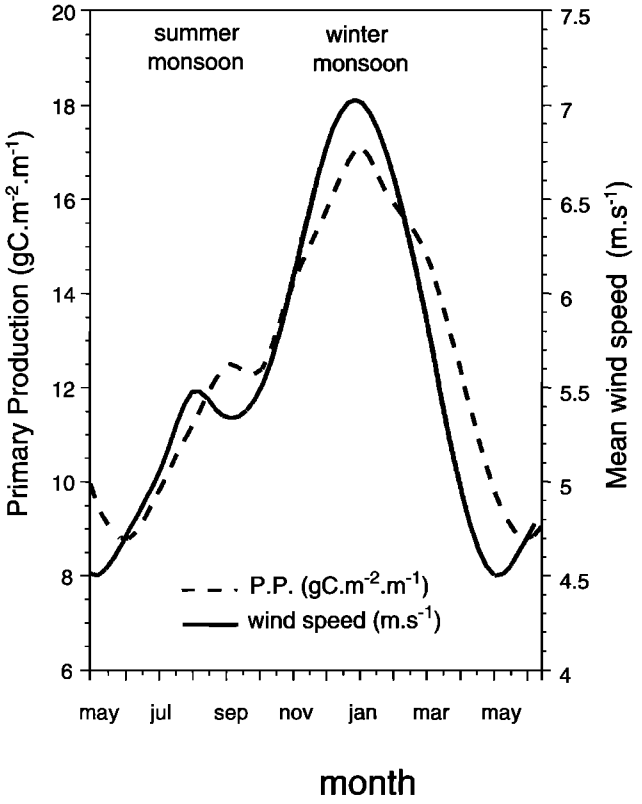

Figure 2. Wind strength in Sulu Sea at 10°N (Comprehensive Ocean-Atmosphere Data Set (COADS) Atlas) and estimated monthly primary production at the same location from *Antoine and Morel* [1996].

The average sedimentation rate is ~10.5 cm kyr^{-1}, with maxima during glacial stage 2 of 34 cm kyr^{-1}. For example, the sedimentation rate during the stage 3 is ~30 cm kyr^{-1}, which allows a 70 year resolution (2 cm sampling). A hiatus occurs between 30 and 22 ka (Figure 3). The sedimentation rates are coherent with other records; that is, they are increased during glacial periods and lower during interglacial stages [e.g., *Chen and Huang*, 1998]. Reduced benthic mixing due to dysaerobic conditions in the Sulu Sea lessens the bioturbation smoothing effect [*Kuehl et al.*, 1993]. The sharp transition in the coccolith record at 14.55 ka, occurs within 2 cm, another argument for a weak bioturbation effect.

3.2. Signal analysis

3.2.1. Spectral analysis. To extract the significant periodicities contained in the PP signal, we performed spectral analysis using different algorithms (Blackman-Tukey, maximum entropy, and multitaper methods) provided in the package Analyseries [*Paillard et al.*, 1996]. The comparison of these different methods allows the discrimination of spurious results due to biases of a particular method. We present only the multitaper method (MTM) results here. The MTM is able to detect low-amplitude oscillations in relatively short time series with a high degree of statistical significance [*Thomson*, 1982]. The statistical significance reported in this work is computed using a Fisher test (F test). This F test is performed on the amplitude to analyze the harmonic oscillations assuming that the signal contains periodic and separated components [*Yiou et al.*, 1997].

3.2.2. Singular-spectrum analysis. Singular-spectrum analysis (SSA) is designed to extract the information contained in a short, nonstationary, and noisy signal [*Vautard and Ghil*, 1989]. This method is based on the computing of empirical orthogonal functions in the time domain. SSA can give insight into the dynamics of the underlying system that generates the signal. Using data-adaptive filters which are not period dependant, SSA allows the separation of the noise from the trend and the deterministic oscillations of the signal.

3.3. *Florisphaera profunda*: A Paleoproductivity Marker

The coccolithophoridae (Prymnesiophycaea) are phytoplanktonic organisms that live in the oceanic photic zone. They are very sensitive to variations in light and nutrient availability, which are both depth dependent. The lower photic zone is darker and richer in nutrients than the upper photic zone. In the tropical ocean the lower photic zone coccolithophoridae community is dominated by *Florisphaera profunda* associated with *Gladiolithus flabellatus* and *Algirosphaera robusta*, while most of the other species live in the upper photic zone [*Okada and Honjo*, 1973].

When the nutricline is shallow, the upper photic zone species dominate the coccolith community, whereas when the nutricline is deeper, the relative proportion of lower photic community is more important. The depth of the nutricline in the low-latitude open ocean is mainly driven by wind intensity. When winds are strong, the upper layers are well mixed, and the nutrients are upwelled into the upper photic zone. Inversely, when wind stress decreases, the mixing is less effective, and the photic zone is depleted in nutrients. This depth relationship between coccolithophorid communities was successfully used by *Molfino and McIntyre* [1990] to monitor changes in the nutricline depth and has been calibrated to primary productivity by *Beaufort et al.* [1997] for paleoproductivity reconstructions.

The relationship between the *Florisphaera profunda* ratio and primary production has already been quantified by *Beaufort et al.* [1997] with the following equation:

$$y = 617 - [279\log(x+3)],$$

where y is the yearly PP (g C m^{-2} yr^{-1}) and x is the percent Fp. This equation is based on Indian Ocean low-latitude core tops. We assume that the coccolithophorids' assemblage distributions are homogenous in the intertropical zone. The variations of Fp are in agreement with other paleoproductivity proxies [*Beaufort et al.*, 1997].

4. Results

The present annual PP in the Sulu Sea is 148 g C m^{-2} yr^{-1} [*Antoine and Morel*, 1996], which is close to the average reconstructed PP over the last 200 kyr of 135 g C m^{-2} yr^{-1}. The PP (data are accessible at http://www.cerege.fr and at ftp://ftp.noaa.ngdc.gov/paleo) oscillates during the last 200 kyr between 81 and 223 g C m^{-2} yr^{-1} (Figure 3).

4.1. Glacial-Interglacial Variations

On a glacial-interglacial timescale, PP increases during glacial periods and decreases during interglacials (Figure 3). PP is moderately correlated (r^2 = 0.49) with the ice volume curve (SPECMAP stack of *Imbrie et al.* [1984]). This is shown by the spectral analysis of the paleoproductivity record, which contains orbital frequency peaks of Milankovitch theory (i.e., 1/100 kyr, 1/41 kyr, and ~1/20 kyr) (Figure 4) and confirmed by cross-spectral analysis between the PP and the SPECMAP stack (not shown). This orbital forcing explains about half of the variance of the PP record. Half of

Table 1. Radiocarbon Ages and Tie Points From the SPECMAP Stack Used in MD97-2141 Chronology[a]

Depth in Core, cm	AMS ^{14}C Age	Error [b]	Calendar Age, years	Species/Age Model	Accession Number
1	4,560	±50	4,798	*G. ruber* (white)	OS-16971
10.5	4,210	±40	4,286	*G. ruber* (white)	OS-16926
14	4,740	±40	4,962	*G. ruber* (white)	OS-16410
29	4,700	±55	4,873	*G. ruber* (white)	OS-16972
59	6,020	±40	6,416	*G. sacculifer* (w/out sac)	OS-16411
73	6,810	±55	7,274	*G. sacculifer* (w/out sac)	OS-16973
85	6,830	±90	7,295	*G. sacculifer* (w/out sac)	OS-18401
94	8,850	±55	9,455	*G. sacculifer* (w/out sac)	OS-16974
99	10,700	±90	12,152	*G. sacculifer* (w/out sac)	OS-16975
120	93,80	±160	10,001	*G sacculifer* (w/out sac)	OS-16977
150	10,200	±80	11,045	*G. ruber* (white)	OS-16978
158	10,250	±120	11,153	*G sacculifer* (w/out sac)	OS-16980
162	10,750	±50	12,228	*G. sacculifer* (w/out sac)	OS-16979
205.5	11,750	±130	13,258	*G. sacculifer* (w/out sac)	OS-17238
212	12,350	±65	13,931	*G. ruber* (white)	OS-16412
226.5	13,000	±95	14,796	*G. ruber* (white)	OS-16970
244	14,100	±70	16,422	*G. ruber* (white)	OS-16413
269	14,750	±70	17,200	*G. ruber* (white)	OS-16361
282	15,100	±90	17,591	*G. sacculifer* (w/out sac)	OS-17913
339	17,150	±140	19,749	*G. ruber* (white)	OS-17914
368	17,650	±85	20,430[c]	*G. ruber* (white)	OS-22672
400	18,850	±140	21,847[c]	*G sacculifer* (w/out sac)	OS-17916
440	28,000	±130	32,101[c]	*G. sacculifer* (w/out sac)	OS-17882
487	30,900	±260	35,146[c]	*G. ruber* (white)	OS-17912
506.5	33,000	±310	37,290[c]	*G. sacculifer* (w/out sac)	OS-17917
543	33,600	±590	37,893[c]	*G sacculifer* (w/out sac)	OS-17911
553	34,300	±390	38,790[c]	*G. sacculifer* (w/out sac)	OS-17915
594	36,900	±460	41,134[c]	*G. sacculifer* (w/out sac)	OS-17918
920			59,000	SPECMAP	
1150			71,000	SPECMAP	
1190			80,000	SPECMAP	
1400			99,000	SPECMAP	
1450			109,000	SPECMAP	
1540			115,000	SPECMAP	
1650			131,000	SPECMAP	
1790			146,000	SPECMAP	
1860			151,000	SPECMAP	
2000			171,000	SPECMAP	
2200			182,000	SPECMAP	

[a] See *Dannenmann et al.* [1998] and *Oppo et al.* [1998].

[b] Error is given in 1σ.

[c] Calendar ages have been calculated using a 400 year reservoir correction and applying the *Stuiver and Braziunas* [1993] calibration curve for samples younger than 20,000 calendar year in age and a U/Th calibration curve for the samples older than 20,000 calendar years [*Bard et al.*, 1993].

the variance of the PP time series remains to be explored in the sub-Milankovitch timescale.

4.2. Sub-Milankovitch Dynamics

4.2.1. Bolling/Allerod and the Younger Dryas event. The last deglaciation is marked by the Younger Dryas event, which interrupts the global warming trend in the Northern Hemisphere. The Younger Dryas seems to be at least hemispheric in extent and has been already described in the Sulu Sea [*Kudrass et al.*, 1991; *Linsley and Thunell*, 1990]. The Younger Dryas event is also present in the MD97-2141 δ^{18}O record between 13.5 and 11.5 ka (Figure 3). The paleoproductivity record inferred from Fp is characterized by an abrupt decrease at 14.55 ka (from 170 to ~125 g C m^{-2} yr^{-1}) to a plateau until 11.5 ka, followed by another decrease to 100 g C m^{-2} yr^{-1}.

We interpret this PP record to indicate a sharp decrease of the East Asian winter monsoon strength after 14.55 kyr. A similar abrupt transition at 14.5 ka is recorded in the alkenone-sea surface temperature (SST) record of the meridional South China Sea as a 1.5°C step [*Pelejero et al.*, 1999a]. Greenland Ice Core Project (GRIP) and Greenland Ice Sheet Project 2 (GISP2) isotopic records also display an abrupt warming at ~14.5 ka. This abrupt warming seems to be at least hemispheric [*Bard et al.*, 1997]. The sea level rise (meltwater pulse (MWP) Ia of *Fairbanks* [1989]) was invoked by *Pelejero et al.* [1999c] to account for the thermal and terrigenous input changes in the South China Sea. However, the abruptness of the PP change (<200 years) is not easily attributable to the flooding of the Sundaland. An abrupt drop in the East Asian winter monsoon intensity can explain this PP change in a more plausible manner.

The interpretation of the Younger Dryas event in the Sulu Sea is still controversial. Two main hypotheses were summarized by *Anderson and Thunell* [1993]: either it reflects a cooling event or it is due to a change in the δ^{18}O of seawater. Modern analog technique reconstruction of SST with planktonic foraminifera does not record enough SST difference during the Younger Dryas to account for the observed isotopic shift [*Thunell and Miao*, 1996]. So the enrichment is probably due to changes in seawater isotopic composition during the Younger Dryas. The origin of this change is still being debated as an oceanic source [*Duplessy*

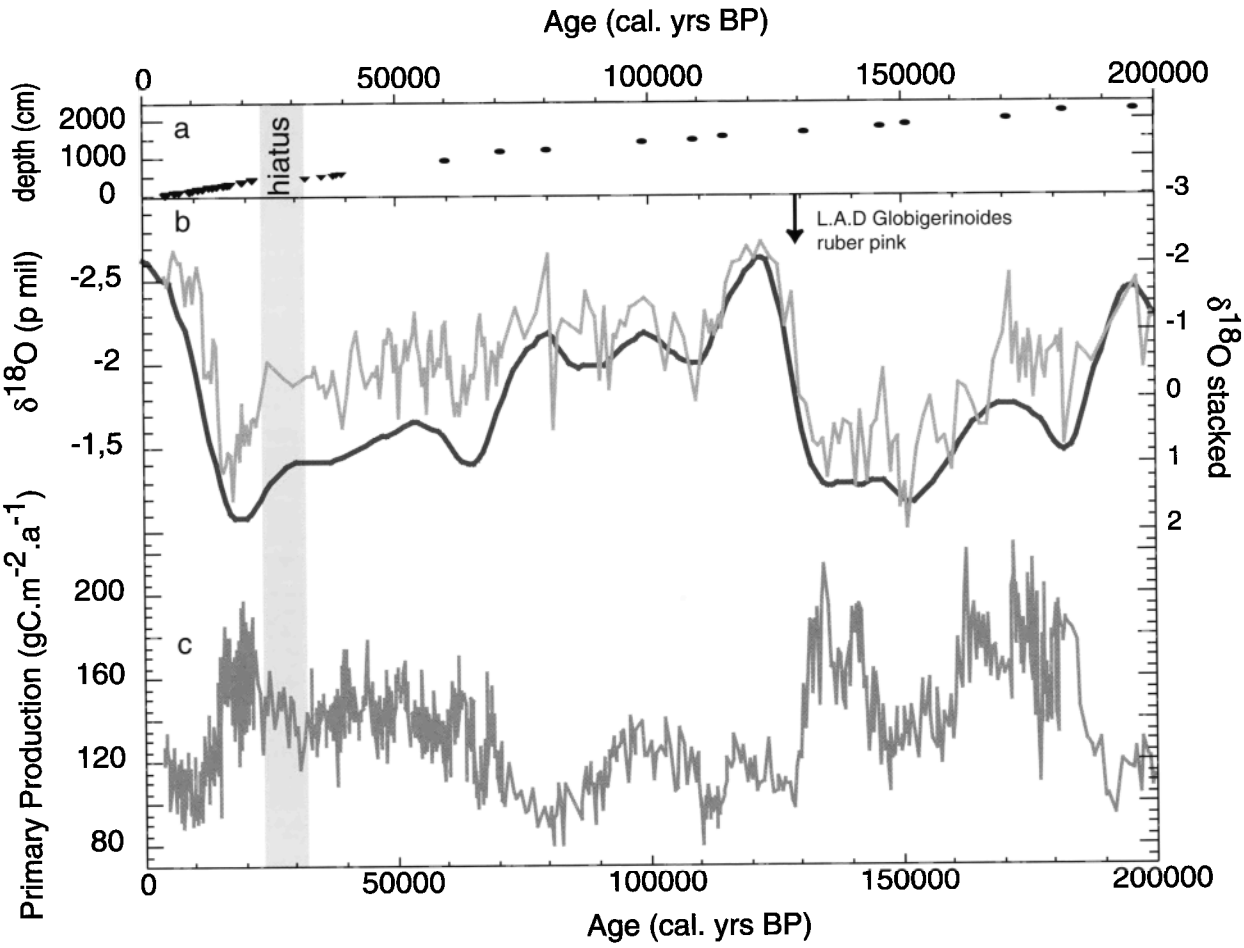

Figure 3. (a) Position of accelerator mass spectrometry (AMS) dates on planktonic foraminifera converted in calendar ages (small triangles) and the SPECMAP tie points used in the stratigraphy (solid circles). Note the hiatus between 400 and 440 cm (shaded area). (b) MD97-2141 $\partial^{18}O$ planktonic foraminifera results at 10 cm intervals (shaded line) compared with the SPECMAP stacked deep-ocean record (thick solid line). (c) MD97-2141 primary productivity (PP) as reconstructed from the coccolithophorid record.

et al., 1991] or an atmospheric variation [*Anderson and Thunell*, 1993].

The PP plateau during the Allerod and the Younger Dryas is similar to the warming recorded by alkenones records from the cores 17961 and 17964 in the South China Sea (SCS) [*Pelejero et al.*, 1999a, 1999b]. The Younger Dryas–Allerod SST difference in the SCS is 0.4°C. This corresponds to an increase of ~0.1‰ of the foraminiferal $\delta^{18}O$, 20% of the 0.5‰ change observed in Sulu Sea sediments [*Linsley*, 1996]. Our PP record strengthens the argument that East Asian winter monsoon dynamics during Younger Dryas were not significantly different from the Allerod because of the small measured change in the PP record between the Allerod and the Younger Dryas. Thus the change in planktonic foraminifera $\delta^{18}O$ composition in the Sulu Sea between the Allerod and the Younger Dryas seems to be mainly due to an isotopic variation in ocean water linked to salinity, after a major change in atmospheric processes 14.5 kyr ago, during the Bolling.

4.2.2. Millennial-scale PP events during MIS 3. The Heinrich events in the North Atlantic have been correlated to short increases of the East Asian winter monsoon dynamics [*Chen et al.*, 1997; *Porter and Zhisheng*, 1995]. In order to compare the millennial variations in the North Atlantic and the PP variations in the Sulu Sea we smoothed the PP record with a 2 kyr average moving window and resampled at a 100 year time step (Figure 5). This 2 kyr window keeps only the variance at the millennial and longer timescales and attenuates the century-scale variations. During the last 80 kyr the PP record reveals eight events numbered PP1-PP8, some of which may be synchronous with North Atlantic environmental changes (Figure 5). The first one (PP1) at ~8.3 kyr ago is in phase with the early to middle Holocene transition period [*Alley et al.*, 1997]. PP2 matches with Heinrich Event 1 (HE1). PP3 occurs during the Last Glacial Maximum. PP4 seems to correlate with HE4. PP5 and PP6 do not match with any major Heinrich Events, and HE5 is being intercalated between these two PP increases. However, PP5, at ~44 ka is correlated to an increase of the winter monsoon strength recorded in paleoloess from China, dated between 43.3 and 45.2 kyr BP (PL7 of *Chen et al.* [1997]). PP7 could be related to HE6. PP8 does not match any Heinrich Event. *Chen et al.* [1997] also describe two events at 59.2–66.2 ka (PL9) and 68.6–71.2 ka (PL10), which may correlate with PP7 and PP8 given age model uncertainties. In conclusion, all PP maxima in the Sulu Sea can be correlated with Chinese loess events and notably events PP5 and PP8 may correspond only with the Chinese loess record. Therefore we conclude that these regional

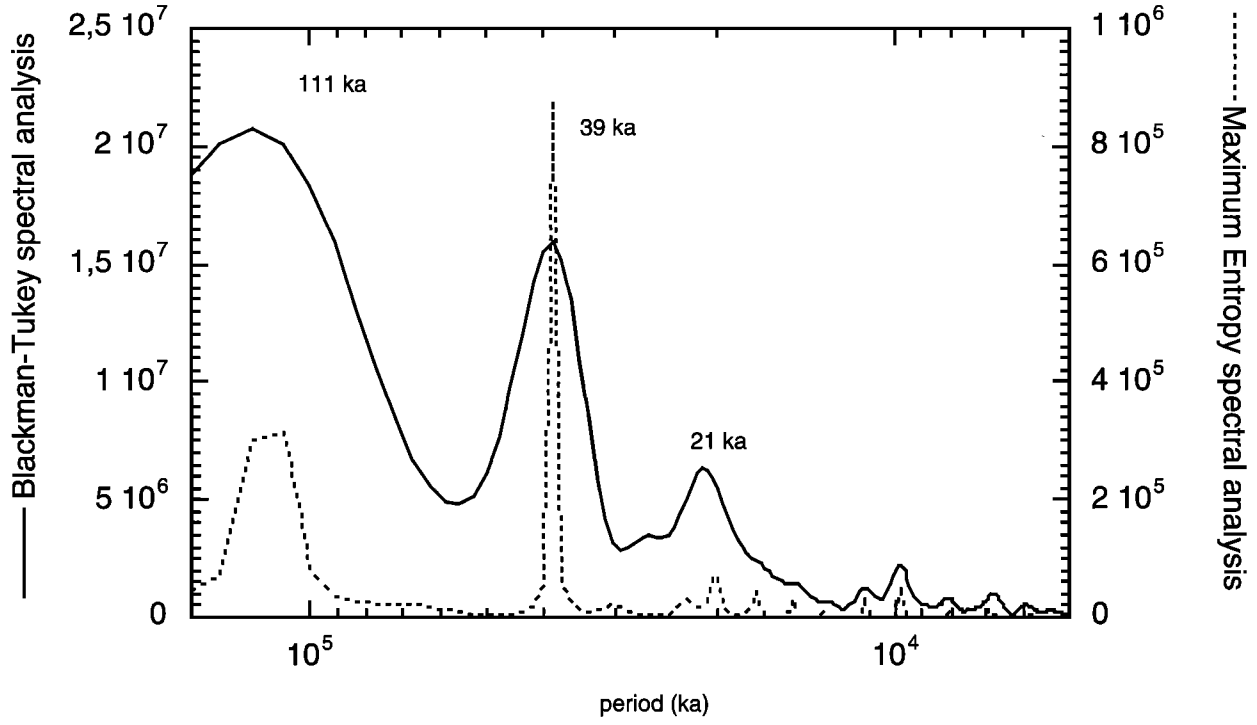

Figure 4. Spectral analysis of the MD97-2141 PP record between 4.1 and 200 ka. Three peaks appear in the spectral analysis computed using the Blackman-Tukey algorithm (solid line) and the maximum entropy algorithm (dotted line), which correspond to orbital frequencies of the Milankovitch theory.

events are indicative of significant changes in the East Asian winter monsoon dynamics. PP1, PP2, PP4, and PP7 match clearly with North Atlantic Heinrich Events. In stage 3, uncertainties in the age model that cannot be smaller than ±2 kyr may explain the relative discrepancy between PP5 or PP6 and HE5 but cannot account for the occurrence of supplementary peaks (PP5 or PP6 and PP8). Our data indicate that the dynamics of the East Asian winter monsoon is not directly linked with the major iceberg discharges in the North Atlantic as stated by *Porter and Zhisheng* [1995]. The East Asian winter monsoon exhibits higher-frequency dynamics than that of the main HE. However, it remains to be determined if a common dynamic is present between the high- and the low-latitude records that is not linked with major icebergs discharges. We next compare the Dansgaard–Oeschger cycles recorded in the Greenland ice core records with our PP record from the Sulu Sea.

To evaluate Dansgaard–Oeschger scale variability, we performed SSA on the Sulu Sea PP and on the GRIP $\delta^{18}O$ records to examine the relationships between Greenland climate and East Asian winter monsoon dynamics. For this analysis, we resampled the two records at 200 year time intervals after interpolation. We computed SSA with the Vautard-Ghil autocovariance estimator embedded in 20 dimensions corresponding to 2000 years. The first principal component (PC) in the two records describes the long-term trend, and the second PC shows millennial dynamics (Figure 6 and Table 2). There is a good agreement between the two PC2 records of millennial dynamics in PP and temperature in Greenland during the last 70 kyr. PP increases in the Sulu Sea when temperatures in Greenland decrease. Cross-spectral analysis indicates high coherency between the PC2 of PP and the PC2 of GRIP for the ~6 and 3.5 kyr frequency bands with phases of ~160° and of 140°, which is indicative of the opposite phase described above. This phase relationship is well constrained for the deglaciation by ^{14}C ages. The phase cannot be further investigated because of limited synchronization between the ice core records and the marine records inherent to differences in established chronologies.

A strengthening of the East Asian winter monsoon during the glacial stages is compatible with the conclusions of several studies already carried out in this area [*Chen and Huang*, 1998; *Wang et al.*, 1999]. It corresponds to a strengthening of the Hadley cell between the Western Pacific Warm Pool Low and the Siberian High. This mode of atmospheric circulation is compatible with last glacial stage simulations [*Kutzbach et al.*, 1993]. The Siberian Highs are directly connected to the Ferrel cells, which influence the Greenland and Asian climates. This teleconnection should operate via the coupling of these two cells (Ferrel and Hadley) during the winter.

In conclusion, the lack of a systematic correlation between the Sulu Sea PP and HE indicates that iceberg discharges in the North Atlantic and the East Asian winter monsoon follow different dynamics. However, the correlation between the Greenland climate PC2 and the East Asian winter monsoon PC2 indicates that similar millennial-scale climate variability affects both the Greenland and the Western Pacific climates.

4.3. Analysis in the Frequency Domain (Suborbital Frequencies)

Three time slices were defined to explore high-frequency cycles in the PP record. The first one, from 22 to 4.1 ka, spans the whole deglaciation. The second one, from 60 to 30 ka, includes most of stage 3. The third one, from 160 to 130 ka, corresponds to the end of stage 6. The PP records were detrended in each segment using a ninth-order polynomial for the deglaciation, a fourth-order polynomial for stage 6, and a linear detrend for stage 3 (Figure 7c). The three records show variance peaks at periods of ~6, 3.5, and 2.4 kyr and between 1780 and 1200 years with a mean at 1500 years (Figure 7e–7g). The spectral peaks could be related to the age

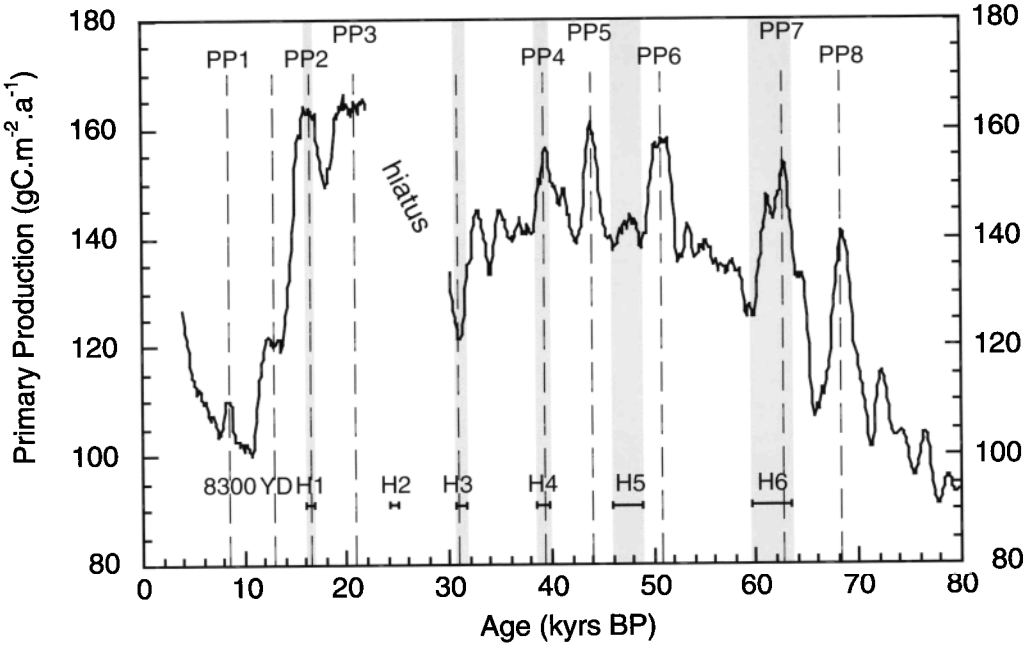

Figure 5. MD97-2141 primary productivity versus calendar age (solid line) smoothed with a 2 kyr moving average window. Between 22 and 30 calendar kyr B.P., a hiatus exists in the sediment record identified with ^{14}C dates (shaded area). The major peaks in PP are numbered from 1 to 8. The Younger Dryas and timing of Heinrich Events in the North Atlantic (shaded area) are shown in toward bottom. The ages for these events are from *Bard* [1998] for the Younger Dryas, *Thouveny et al.* [2000] for North Atlantic Heinrich Events 1–4, and *Chapman and Shackleton* [1998] for the chronology of H5 and H6.

model. However, changing the age model from polynomial fits to linear fits does not change the periods of the peaks >100 years, and the relative timing of the peaks is kept. Thus the spectral peaks seem to be robust features of the signal with this current age model.

4.3.1. The ≈1.5 kyr cycle. For the time slice from 4.1 to 22 ka the most significant peak occurs at 1.38 kyr (significance of 93%). In the 30–60 ka time slice, two peaks occur at 1.54 kyr (98.5%) and 1.2 kyr (99.8%). In the last time slice the peak is at 1.48 ka (99%). The strongest periods are all around 1.4–1.5 kyr, and the occurrence in three different time-slices indicates probably a common origin and an almost stationary signal across different climatic conditions.

4.3.2. The ≈2.4 kyr cycle. In the 4.1–22 ka time slice, two minor peaks occur (2.58 and 2.17 kyr), but they are not significant. In the 30–60 ka time slice the prominent peak occurs at 2.32 kyr (significance of 79.8%). In the 130–160 ka time slice a significant peak is at 2.43 kyr (96%). The period of 2.4 kyr seems also stationary, but its strength varies through time. It is more marked during the glacial stages and may correspond to ice volume forcing.

4.3.3. The ≈4.2-3.3 kyr cycle. In the time slice from 22 to 4.1 ka the peak is at ~4.2 (significance of 97%). The 30–60 ka time slice peaks at 3.6 kyr (97%), and in the 130–160 ka time slice the significant peak is at 3.36 kyr (86%). The strength of this peak is strong in all the time slices, but the period does not seem to be stationary.

4.3.4. The ≈6 kyr cycle. In the time slice between 4.1 and 22 ka the peak at ~8 kyr is not significant because of the dominant deglaciation signal overprints on the low-frequency band. In the 30–60 ka time slice a peak occurs at 5.7 kyr (significance of 89.9%), and between 130 and 160 ka the significant peak is at 6.7 kyr (92.1%) with another concentration of variance at ~5.06 kyr (90.5%). This frequency is most pronounced during the glacials periods.

5. Discussion: High-Frequency Cycles

Because the frequency of ~6 kyr^{-1} is close to the Heinrich Events' frequency band, we filtered the PP record in this frequency band using a Gaussian filter (bandwidth of 0.1666 $kyr^{-1} \pm 0.03$) (Figure 8a). The resulting PP series clearly shows an amplification during the glacial periods, with minima during interglacials (i.e., Holocene and stage 5: 75–130 ka), and indicates that this frequency seems to be ice volume forced. The amplification could depend on the high-latitude ice volume available for ice rafting events.

A 3.7 kyr cycle has already been reported by *Pestiaux et al.* [1988] in the Indian Ocean. A similar periodicity of 3.3 kyr was also reported by *Sirocko et al.* [1996] in a production record from the Arabian Sea. These authors attributed this frequency band to combination tones of orbital forcing on monsoon dynamics. In the Sulu Sea this period is significant during the MIS3. This period is not very stable in the PP record, oscillating between 3.62 kyr for stage 3 and 3.36 kyr for stage 6. The identification of this period in several paleomonsoon records seems to indicate that this period is significant in Asian monsoon system dynamics. The hypothesis of combination tones related to precessional and to obliquity frequencies, which forces the climate system like a nonlinear oscillator [*Pestiaux et al.*, 1988], could explain the variations of the spectral peaks contained in this frequency band. Even if a nonlinear climatic oscillator predicts only periods >5 kyr [*Le Treut and Ghil*, 1983], the monsoon system by its amplification of insolation forcing could probably generate cycles in this frequency band [*Pestiaux et al.*, 1988].

5.1. The 2.4 kyr Cycle

The PP exhibits a strong 2.4 kyr cycle, especially during the last two glacial stages (MIS 2–3 and 6). This period has already been described in oceanic sediments. *Pestiaux et al.* [1988] observe a 2.3 kyr period in the Indian Ocean hydrography, which

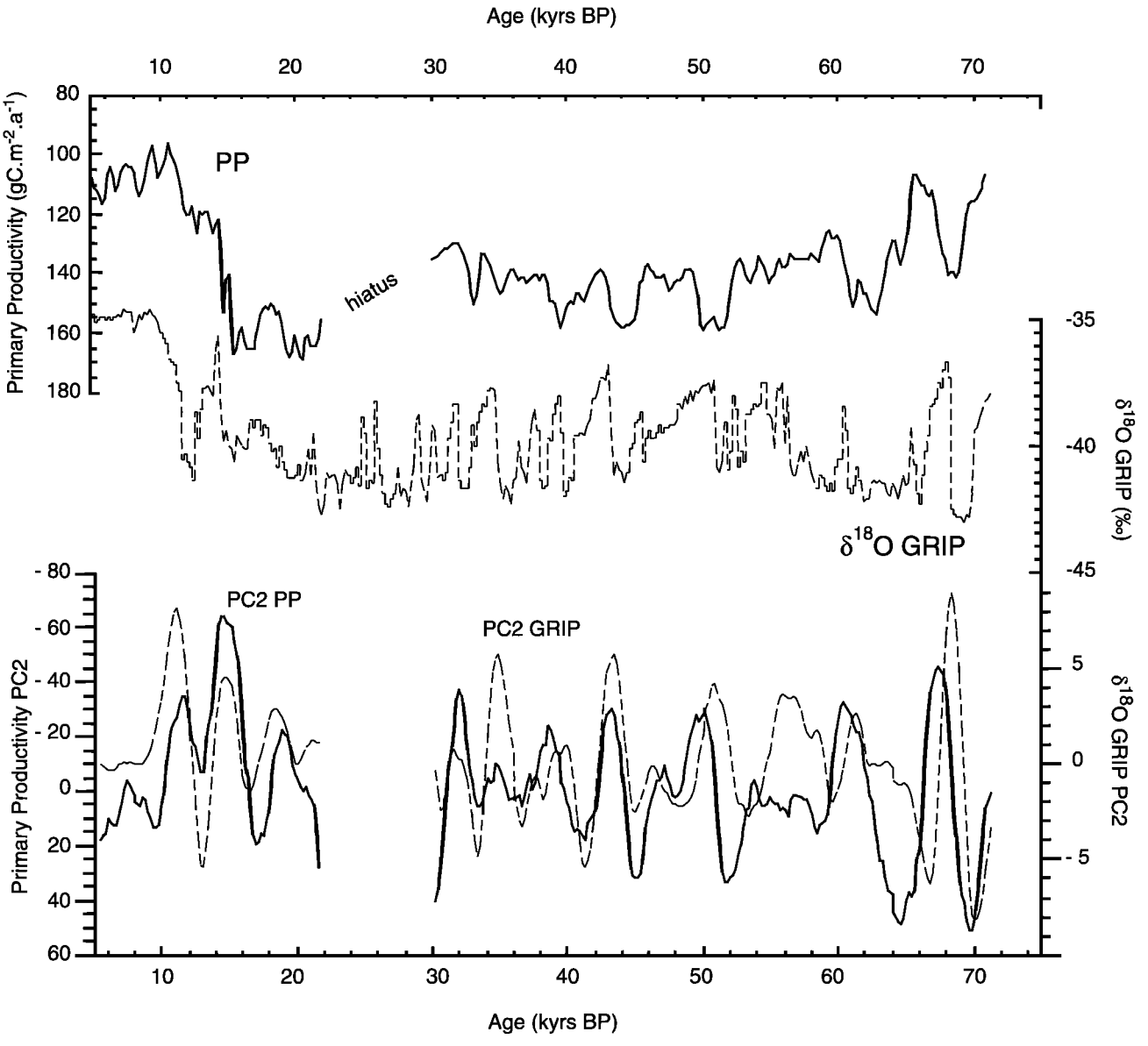

Figure 6. (top) MD97-2141 PP (smoothed; solid line) record versus the $\partial^{18}O$ record of the GRIP ice core (dotted line). (bottom) PC2 of the PP record (solid line) and PC2 of the $\delta^{18}O$ record of GRIP (dotted line) as reconstructed by singular spectrum analysis (SSA), which show similar oscillations. Note that both scales in the bottom panel are inverted compared to the top panel.

was interpreted as a combination tone of the precessional and obliquity cycles, representing an internal but nonlinear response of the monsoon system to solar forcing. This cycle is also present in the atmospheric ^{14}C excess record [*Stuiver and Braziunas*, 1993], which depends on the solar flux (Hallstattzeit cycle [*Damon and Jirikowic*, 1992]) and on the oceanic-atmosphere exchange of ^{14}C. A 2.2 kyr periodicity was also reported in a monsoon record from the Oman margin [*Naidu and Malgrem*,

Table 2. Percent Variance Described by the Principal Components of the Singular-Spectrum Analysis and Mean Periods of the PCs

	PP in Sulu Sea			$\delta^{18}O$ GRIP		
	Described Variance, %	Cumulative Variance, %	Mean Period, years	Described Variance, %	Cumulative Variance, %	Mean Period, years
PC1	82.52	82.52	>8000	67.64	67.64	>8000
PC2	6.76	89.29	6200	13.56	81.21	5500
PC3	2.98	92.28	3690	8.4	89.61	3500
PC4	1.67	93.95	2400	3.45	93.06	2760
PC5	1.15	95.10	1870	1.76	94.83	1870
PCs 6-20	4.9	100	...	6.07	100	...

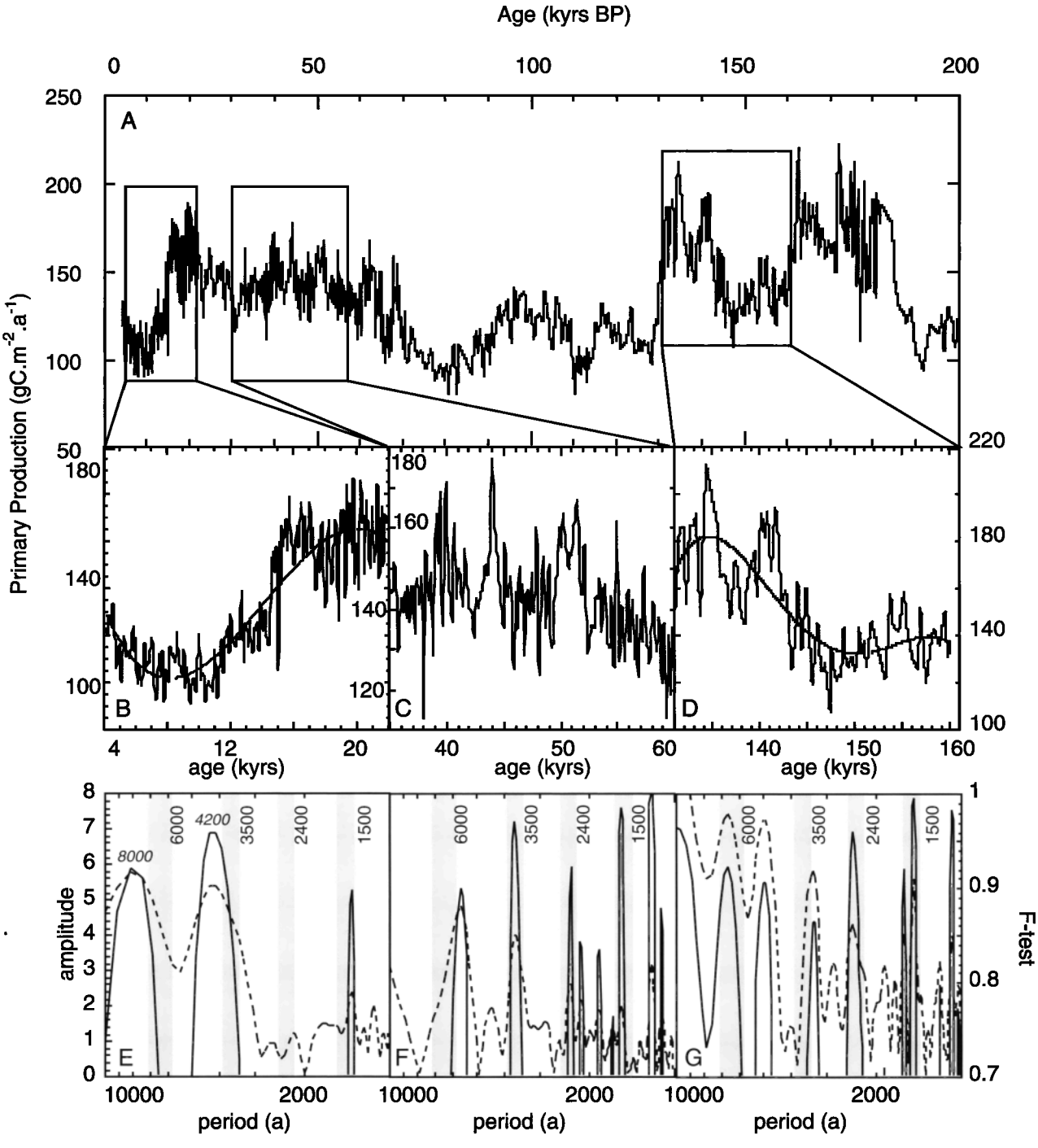

Figure 7. (a) MD97-2141 primary productivity (0–200 ka). Three intervals are enlarged in Figures 7a–7c. (b) From 4 to 22 calendar kyr B.P. A polynomial of third order (thin solid line) was applied to detrend the primary productivity signal (thick solid line) before the multitaper method (MTM) spectral analysis. (c) From 35 to 60 ka. PP (thick solid line) is represented, a linear detrend was performed before spectral analysis. (d) From 130 to 160 ka. A fifth-order polynomial (thin solid line) of the PP (thick solid line) was also subtracted from the PP record before the spectral analysis. (e–g) MTM spectra of the three time windows in Figures 7b, 7c, and 7d, respectively. Line amplitudes (dashed line) and *F* test (estimate of confidence; solid line) are plotted versus period. The shaded areas represent significant frequency bands.

1995], which was attributed to interactions between oceanic circulation changes and atmospheric ^{14}C changes at a 2.3 kyr period. This cycle is not expressed in Termination I of the Sulu Sea PP record. However, it is significant for the glacials stages. The low expression of this cycle in the Sulu Sea during the last termination is perhaps due to the strong overprint of the 1.5 kyr cycle on the PP record. This cycle seems to be stationary throughout this record.

5.2. Pseudo 1.5 kyr Cyclicity

A 1.47 kyr period was first described by *Dansgaard et al.* [1984] in the Camp century $\delta^{18}O$ ice core record. In the Summit ice core (GISP2) the $\delta^{18}O$ and the polar component of a principal component analysis computed on various chemical markers in the ice both show periods ~1.5 kyr [*Mayewski et al.*, 1997]. A 1.47 kyr period was also described by *Bond et al.* [1997] in North Atlantic deep-sea cores during the Holocene and the deglaciation. In Alaska, a lake record contains climatic variations with a 1.5 kyr cycle [*Campbell et al.*, 1998]. These records provide growing evidence for cyclicity of ~1.5 kyr in many high-latitude records. This cycle was also recently linked to fluctuations in continental ice mass during periods of lowered sea level (−45 m below present level) by a simple model of ice dynamics [*Schulz et al.*, 1999]. At lower latitudes the southwest Indian monsoon also shows clear 1.45 kyr cycles in a paleoproductivity record spanning the last deglaciation [*Sirocko et al.*, 1996]. Sirocko et al. speculate that this relationship could be due to subprecessional forcing.

In the Sulu Sea the primary productivity shows clear peaks in a broader 1.5 kyr band (Figure 7). The peak in PP is at 1.38 kyr for the last 22 kyr. For stage 2–3 the major peak is at 1.37 kyr. That ~1.5 kyr cyclicity is also present during stage 6. During the last deglaciation the cycles are well defined. This pseudoperiodicity appears significant in the three time slices, suggesting that it is a pervasive feature of the East Asian winter monsoon dynamics. Our low-latitude record clearly does not record an amplification with increase in the polar continental ice masses (i.e., the sea level does not modulate the envelope of the 1.5 kyr cycle). During the last 160 kyr, eight maxima in the 1.5 kyr envelope were counted, which correspond roughly to the precession period (160/8 = 20 kyr) (Figure 8b). The East Asian monsoon 1.5 kyr cycle thus could be the climatic expression of a combination tone of the orbital insolation frequencies as already expressed by *Pestiaux et al.* [1988] and *Sirocko et al.* [1996]. The pervasive occurrence of this cycle during both glacial and interglacial periods in the subtropics seems to indicate that if a 1.5 kyr climate oscillator exists, a common origin between high and low latitudes is expected for this cyclicity. We suggest that its presence in the Sulu Sea is not forced by high latitudes, as indicated by its presence during stages 1 and 5 in the Sulu Sea and absence in the intervals in the GRIP record [*Stuiver and Braziunas*, 1993]. Further data are necessary to improve the definition of the frequency bands and the geographical extent of these rapid climate cycles.

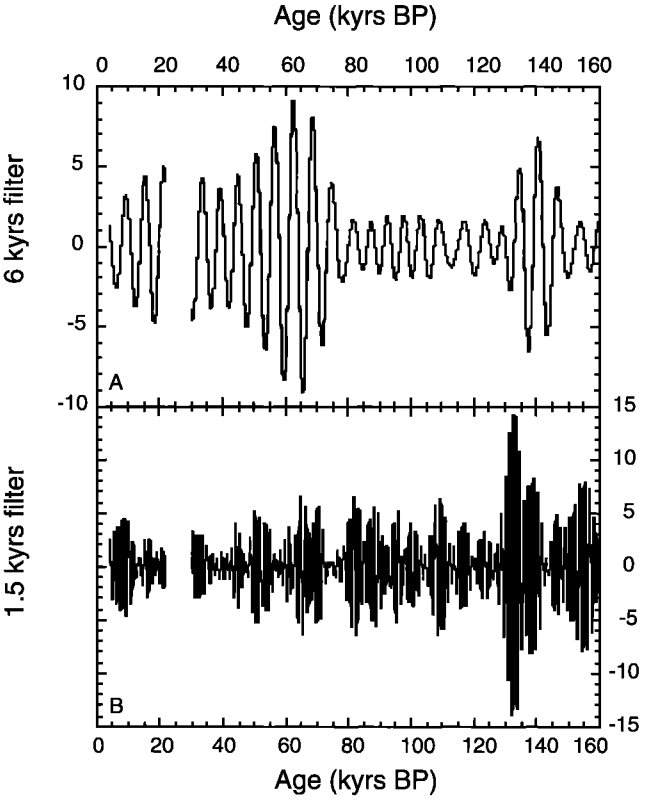

Figure 8. Filtered PP with a Gaussian filter centered on (a) 6000 years and (b) 1500 years. The envelope of the 1500 years filtered signal exhibits a ~20,000 years modulation.

6. Conclusions

We reconstructed primary productivity (PP) from coccoliths in the MD97-2141 core, located in the Sulu Sea during the last 200 kyr.

1. We find that PP increased during the glacial stages, whereas the interglacials are times of lower PP. We attribute this PP change to a strengthening of the East Asian winter monsoon in the Sulu Sea during glacial stages.

2. The PP record indicates that an abrupt decrease in the East Asian winter monsoon occurred 14.55 calendar kyr B.P., followed by a ~2 kyr plateau during both Allerod and Younger Dryas. It shows that changes in the $\delta^{18}O$ record from the Sulu Sea during the Younger Dryas are most likely linked with sea surface salinities changes.

3. The PP record exhibits eight rapid oscillations during the last 70 kyr. Only four PP events are synchronous with Heinrich Events. This implies that the East Asian winter monsoon and North Atlantic iceberg discharges follow different dynamics, and that HE are not systematically forcing increases in the East Asian winter monsoon. However, these PP oscillations appear to correlate with peaks of the East Asian monsoon recorded in the Chinese loess. In the timescale close of the pacing of Dansgaard–Oeschger cycles, singular-spectrum analysis reveals that the PP record in the Sulu Sea can be correlated with the Greenland climate. Therefore a common dynamic, which is not forced by icebergs discharges in the North Atlantic, is present in both high- and low-latitude paleoclimatic records.

4. Four dominant frequencies were isolated in the high-frequency pacing of the East Asian winter monsoon. They occur (1) at ~6 kyr, (2) in a 3.3–4.2 kyr frequency band of unknown origin, (3) in a 2.4 kyr frequency band probably resulting from the coupling between solar flux and oceanic processes, and (4) in a 1.5 kyr band. This ~1.5 kyr pseudoperiodicity is a pervasive feature of the East Asian winter monsoon during the marine stages 1, 3, 5, and 6. The origin of this climatic cyclicity remains unknown, but we suggest that its presence at this site in the low-latitude western Pacific is not forced from the high latitudes.

Acknowledgments. The support of French MENRT, TAAF, CNRS/INSU, and IFRTP to the *Marion-Dufresne* and the IMAGES Program was necessary to perform this work. T.G. was supported by a predoctoral grant of the French Ministère de la Recherche. Financial support from INSU grant to T.G. and L.B. is acknowledged. B.K.L. acknowledges grant OCE 9710156 and technical assistant Stephen Howe. We are indebted to Delia Oppo, who contributed to the collection of the AMS ^{14}C ages at the WHOI-NOSAMS AMS facility and $\delta^{18}O$ data with the NSF grant OCE-9710097, and the technical help of Susan Trimarchi and Luping Zou.

References

Alley, R. B., P. A. Mayewski, T. Sowers, M. Stuiver, K. C. Taylor, and P. U. Clark, Holocene climatic instability: A prominent, widespread event 8200 yr ago, *Geology*, *25*(6), 483–486, 1997.

Anderson, D. M., and R. C. Thunell, The oxygen-isotope composition of tropical ocean surface water during the last deglaciation, *Quat. Sci. Rev.*, *12*, 456–473, 1993.

Antoine, D., and A. Morel, Oceanic primary production, 2, Estimation at global scale from satellite (coastal zone color scanner) chlorophyll, *Global Biogeochem. Cycles*, *10*, 57–70, 1996.

Bard, E., Correlation of accelerator mass spectrometry ^{14}C ages measured in planktonic foraminifera: Paleoceanographic implications, *Paleoceanography*, *3*(6), 635–645, 1988.

Bard, E., Geochemical and geophysical implications of the radiocarbon calibration, *Geochim. Cosmochim. Acta*, *62*(12), 2025–2038, 1998.

Bard, E., M. Arnold, R. G. Fairbanks, and B. Hamelin, ^{230}Th-^{234}U and ^{14}C ages obtained by mass spectrometry on corals, in *Calibration 1993*, edited by M. Stuiver, A. Long, and R. S. Krea, pp. 191–200, Dep. of Geosci., Univ. of Ariz., Tucson, 1993.

Bard, E., F. Rostek, and C. Sonzogni, Interhemispheric synchrony of the last deglaciation inferred from alkenone palaeothermometry, *Nature*, *385*, 707–710, 1997.

Beaufort, L., Y. Lancelot, P. Camberlin, O. Cayre, E. Vincent, F. Bassinot, and L. Labeyrie, Insolation cycles as a major control of equatorial Indian Ocean primary production, *Science*, *278*, 1451–1454, 1997.

Behl, R , and J. P. Kennet, Brief interstadial events in the Santa Barbara basin, NE Pacific, during the past 60 kyr, *Nature*, *379*, 243–246, 1996.

Bond, G., et al., Evidence for massive discharges of icebergs into the North Atlantic Ocean during the last glacial period, *Nature*, *360*, 245–249, 1992.

Bond, G., W. Showers, M. Chezebiet, R. Lotti, P. Almasi, P. deMenocal, P. Priore, H. Cullen, I. Hajdas, and G. Bonani, A pervasive millennial scale cycle in North-Atlantic Holocene and glacial climates, *Nature*, *278*, 1257–1266, 1997.

Campbell, I. D., C. Campbell, M. J. Apps, N. W. Rutter, and A. B. G. Bush, Late Holocene ca. 1500 yr climatic periodicities and their implications, *Geology*, *26*(5), 471–473, 1998.

Chapman, M. R., and N. J. Shackleton, Millennial-scale fluctuations in North Atlantic heat flux during the last 150,000 years, *Earth Planet Sci. Lett.*, *159*, 57–70, 1998.

Chen, F. H., J. Bloemendal, J. M. Wang, J. Li, and L. Oldfield, High-resolution multi-proxy climate records from Chinese loess: Evidence for rapid climatic changes over the last 75 kyr, *Palaeogeogr. Palaeoclimatol. Palaeoecol.*, *130*, 323–335, 1997.

Chen, M. T., and C. Y. Huang, Ice-volume forcing of the winter monsoon climate in the South China Sea, *Paleoceanography*, *13*(6), 622–633, 1998.

Cortijo, E., L. Labeyrie, M. Elliot, E. Balbon, and N. Tisnerat, Rapid climatic variability of the North Atlantic Ocean and global climate: A focus of the IMAGES program, *Quat. Sci. Rev.*, *19*, 2000.

Damon, P. E., and J. L. Jirikowic, The sun as a low-frequency harmonic oscillator, *Radiocarbon*, *34*(2), 199–205, 1992.

Dannenmann, S., B. K. Linsley, D. W. Oppo, and R. D. Norris, Centennial resolution isotopic record from the Sulu Sea: 10 kyr to 60 kyr, *Eos Trans. AGU*, *79*(45), Fall Meet. Suppl., F454, 1998.

Dansgaard, W., S. J. Johnsen, H. B. Clausen, N. Dahl-Jensen, N. Gundestrup, and C. U. Hammer, North Atlantic climatic oscillations revealed by deep Greenland ice cores, in *Climate Processes and Climate Sensitivity, Geophys Monogr. Ser*, vol. 29, edited by J. E. Hansen and T. Takahashi, pp. 288–298, AGU, Washington, D. C., 1984.

Dansgaard, W., et al., Evidence for general instability of past climate from a 250 kyr ice-core record, *Nature*, *364*, 218–220, 1993.

Duplessy, J.-C., E. Bard, M. Arnold, N. J. Shackleton, J. Duprat, and L. Labeyrie, How fast did the ocean-atmosphere system run during the last deglaciation?, *Earth Planet. Sci. Lett.*, *103*, 27–40, 1991.

Fairbanks, R. G., A 17000 year glacio-eustatic sea-level record: Influence of glacial melting rates on the Younger Dryas event and deep-ocean circulation, *Nature*, *342*, 637–642, 1989.

Heinrich, H., Origin and consequences of cyclic ice rafting in the northeast Atlantic during the past 130 000 years, *Quat. Res.*, *29*, 142–152, 1988.

Imbrie, J., J. D. Hays, D. G. Martinson, A. McIntyre, A. C. Mix, J. J. Morley, N. G. Pisias, W. L. Prell, and N. J. Shackleton, The orbital theory of Pleistocene climate: Support from a revised chronology of the marine $\delta^{18}O$ record, in *Milankovitch and Climate*, edited by A. L. Berger et al., pp. 269–305, D. Reidel, Norwell, Mass., 1984.

Jouzel, J., Calibrating the isotopic paleothermometer, *Science*, *286*, 910–911, 1999.

Kudrass, H. R., H. Erlenkeuser, R. Vollbrecht, and W. Weiss, Global nature of the Younger Dryas cooling event inferred from oxygen isotope data from Sulu sea cores, *Nature*, *349*, 406–409, 1991.

Kuehl, S. A., T. G. Fuglseth, and R. C. Thunell, Sediment mixing and accumulation rates in the Sulu and the South China Seas: Implications for organic preservation in deep-sea sediments, *Mar Geol.*, *111*, 15–35, 1993.

Kutzbach, J. E., P. J. Guetter, P. J. Behling, and R. Selin, Simulated climatic changes: Results of the COHMAP climate-model experiments, in *Global Climates Since the Last Glacial Maximum*, edited by H. E. Wright, Jr. et al., pp. 24–93, Univ. of Minn. Press, Minneapolis, 1993.

Le Treut, H., and M. Ghil, Orbital forcing, climatic interactions and glaciations cycles, *J. Geophys. Res* , *88*, 5167–5190, 1983.

Linsley, B. K., Oxygen-isotope record of sea-level and climate variations in the Sulu Sea over the past 150,000 years, *Nature*, *380*, 234–237, 1996.

Linsley, B. K., and R. C. Thunell, The record of deglaciation in the Sulu Sea: Evidence for the Younger Dryas event in the tropical western Pacific, *Paleoceanography*, *5*(6), 1025–1039, 1990.

Linsley, B. K., R. C. Thunell, C. Morgan, and D. Williams, Oxygen minimum expansion in the Sulu Sea, western equatorial Pacific, during the last glacial low stand of sea level, *Mar. Micropaleontol.*, *9*, 395–418, 1985.

Mayewski, P. A., L. D. Meeker, M. S. Twickler, S. Whitlow, Q. Yang, W. B. Lyons, and M. Prentice, Major features and forcing of high-latitude Northern Hemisphere atmospheric circulation using a 110,000-year long glaciogeochemical series, *J. Geophys. Res.*, *102*, 26,345–26,366, 1997.

McGregor, G. R., and S. Nieuwolt, *Tropical Climatology*, 339 pp., John Wiley, New York, 1998.

Miao, Q., R. Thunell, and D. M. Anderson, Glacial-Holocene carbonate dissolution and sea surface temperatures in the South China and Sulu Seas, *Paleoceanography*, *9*(2), 269–290, 1994.

Mix, A., Influence of productivity variations on long-term atmospheric CO_2, *Nature*, *337*, 541–544, 1989.

Molfino, B., and A. McIntyre, Precessional forcing of nutricline dynamics in the equatorial Atlantic, *Science*, *249*, 766–769, 1990.

Naidu, P. D., and B. A. Malgrem, A 2,200 years periodicity in the Asian monsoon system, *Geophys. Res. Lett.*, *22*(17), 2361–2364, 1995.

Nair, R. R., V. Ittekkot, S. J. Manganini, V. Ramaswamy, B. Haake, E. T. Degens, B. N. Desai, and S. Honjo, Increased particle flux to the deep ocean related to monsoons, *Nature*, *338*, 749–751, 1989.

Okada, H., and S. Honjo, The distribution of oceanic coccolithophorids in the Pacific, *Deep Sea Res.*, *20*, 355–374, 1973.

Oppo, D. W., B. K. Linsley, S. Dannenmann, and R. D. Norris, Centennial-to-millennial scale variability recorded in Holocene sediments from the Sulu and South China Seas, *Eos Trans AGU*, *79*(45), Fall Meet. Suppl., F454, 1998.

Paillard, D., L. Labeyrie, and P. Yiou, Macintosh performs time-series analysis, *Eos Trans. AGU*, *77*(39), 379, 1996.

Patterson, R. T., and E. Fishbein, Re-examination of the statistical methods used to determine the number of point counts needed for micropaleontological quantitative research, *J. Paleontol.*, *63*(2), 245–248, 1989.

Pelejero, C., J. O. Grimalt, S. Heilig, M. Kienast, and L. Wang, High-resolution U^{k}_{37} temperature reconstructions in the South China Sea over the past 220 kyr, *Paleoceanography*, *14*(2), 224–231, 1999a.

Pelejero, C., J. O. Grimalt, M. Sarnthein, L. Wang, and J. A. Flores, Molecular biomarker record of sea-surface temperature and climatic change in the South China Sea during the last 140,000 years, *Mar. Geol.*, *156*, 109–121, 1999b.

Pelejero, C., M. Kienast, L. Wang, and J. O. Grimalt, The flooding of Sundaland during the last deglaciation: Imprints in hemipelagic sediments from the southern South China Sea, *Earth Planet. Sci. Lett.*, *171*, 661–671, 1999c.

Pestiaux, P., I. Van Der Mersch, A. Berger, and J.-C. Duplessy, Paleoclimatic variability at frequencies ranging from 1 cycle per 10,000 years to 1 cycle per 1000 years—Evidence for non-linear behaviour of the climate system, *Clim. Change*, *12*, 9–37, 1988.

Porter, S. C., and A. Zhisheng, Correlation between climate events in the North Atlantic and China during the last glaciation, *Nature*, *375*, 305–308, 1995.

Schulz, H., U. von Rad, and H. Erlenkeuser, Correlation between Arabian Sea and Greenland climate oscillations of the past 110,000 years, *Nature*, *393*, 54–57, 1998.

Schulz, M., W. H. Berger, M. Sarnthein, and P. M. Grootes, Amplitude variations of 1470-year climate oscillations during the last 100,000 years linked to fluctuations of continental ice mass, *Geophys. Res Lett.*, *26*(22), 3385–3388, 1999.

Sirocko, F., D. Garbe-Sch—nberg, A. McIntyre, and B. Molfino, Teleconnections between the subtropical monsoons and high-latitude climates during the last deglaciation, *Science*, *272*, 526–529, 1996.

Stuiver, M., and T. F. Braziunas, Sun, ocean,

climate and atmospheric $^{14}CO_2$: An evaluation of causal and spectral relationships, *Holocene*, *3*(4), 289–305, 1993.

Stuiver, M., and P. J. Reimer, Calib Rev. 3, *Radiocarbon*, *35*, 215–230, 1993.

Thompson, P. R., A. W. H. Bé, J.-C. Duplessy, and N. C. Shackleton, Disappearance of pink-pigmented *Globigerinoides ruber* at 120,000 yr BP in the Indian and Pacific Oceans, *Nature*, *280*, 554–558, 1979.

Thomson, D. J., Spectrum estimation and harmonic analysis, *IEEE Proc.*, *70*, 1055, 1982.

Thouveny, N., E. Moreno, D. Delanghe, L. Candon, Y. Lancelot, and N. J. Shackleton, Rock-magnetic detection of distal ice rafted debries: Clue for the identification of Heinrich layers on the Portuguese margin, *Earth Planet. Sci. Lett.*, *180*, 61–75, 2000.

Thunell, R. C., and Q. C. Miao, Sea-surface temperature of the western equatorial Pacific during the Younger Dryas, *Quat. Res.*, *46*, 72–77, 1996.

Vautard, R., and M. Ghil, Singular spectrum analysis in nonlinear dynamics, with applications to paleoclimatic time series, *Physica D*, *35*, 395–424, 1989.

Wang, L., M. Sarnthein, H. Erlenkeuser, J. Grimalt, P. Grootes, S. Heilig, E. Ivanova, M. Kienast, C. Pelejero, and U. Pflaumann, East Asian monsoon during the late Pleistocene: high-resolution sediment records from the South China Sea, *Mar Geol.*, *156*, 245–284, 1999.

Wiesner, M. G., L. Zheng, H. K. Wong, Y. Wang, and W. Chen, Fluxes of particulate matter in the South China Sea, in *Particle Flux in the Ocean*, edited by J. Ittekkot et al., pp. 293–312, John Wiley, New York, 1996.

Xiao, J. L., Z. S. An, T. S. Liu, Y. Inouchi, H. Kumai, S. Yoshikawa, and Y. Kondo, East Asian monsoon variation during the last 130,000 years: Evidence from the Loess Plateau of central China and Lake Biwa of Japan, *Quat. Sci. Rev.*, *18*, 147–157, 1999.

Yan, X.-H., C.-R. Ho, Q. Zheng, and V. Klemas, Temperature and size variabilities of the Western Pacific Warm Pool, *Science*, *258*, 1643–1645, 1992.

Yiou, P., K. Fuhrer, L. D. Meeker, J. Jouzel, E. Jansen, and P. A. Mayewski, Paleoclimatic variability inferred from the spectral analysis of Greenland and Antartic ice-core data, *J. Geophys. Res.*, *102*, 26, 441–26, 454, 1997.

Zhang, Y., East Asian winter monsoon: Results from eight AMIP models, *Clim. Dyn.*, *13*(11), 797–820, 1997.

L. Beaufort and T. de Garidel-Thoron, Centre Européen de Recherche et d'Enseignement en Géosciences de l'Environnement, Europôle méditerranéen de l'Arbois, BP 80, Aix-en-Provence cedex 4, 13545 France. (garidel@cerege.fr)

S. Dannenmann and B. K. Linsley, Department of Earth and Atmospheric Sciences, University at Albany, State University of New York, Albany, NY 12222, USA.

(Received June 26, 2000;
revised April 26, 2001;
accepted May 25, 2001.)